Inorganic Chemistry

Article

pubs.acs.org/IC

Role of Axial Base Coordination in Isonitrile Binding and Chalcogen Atom Transfer to Vanadium(III) Complexes

Subhojit Majumdar,[†] Julia M. Stauber,[‡] Taryn D. Palluccio,[§] Xiaochen Cai,[†] Alexandra Velian,[‡] Elena V. Rybak-Akimova,*[,§] Manuel Temprado,*[,∥] Burjor Captain,*[,†] Christopher C. Cummins,*[,‡] and Carl D. Hoff*[,†]

[†]Department of Chemistry, University of Miami, 1301 Memorial Drive, Coral Gables Florida 33021, United States

[‡]Department of Chemistry, Massachusetts Institute of Technology, 77 Massachusetts Avenue, Cambridge, Massachusetts 02139, United States

[§]Department of Chemistry, Tufts University, 62 Talbot Avenue, Medford, Massachusetts 02155, United States

[∥]Department of Analytical Chemistry, Physical Chemistry and Chemical Engineering, Universidad de Alcalá, Ctra. Madrid-Barcelona Km. 33.600, Madrid, 28871, Spain

Supporting Information

ABSTRACT: The enthalpy of oxygen atom transfer (OAT) to V[$(Me_3SiNCH_2CH_2)_3N$], **1**, forming OV[$(Me_3SiNCH_2CH_2)_3N$], **1**−O, and the enthalpies of sulfur atom transfer (SAT) to **1** and V(N[*t*-Bu]Ar)$_3$, **2** (Ar = 3,5-$C_6H_3Me_2$), forming the corresponding sulfides SV[$(Me_3SiNCH_2CH_2)_3N$], **1**−S, and SV(N[*t*-Bu]Ar)$_3$, **2**−S, have been measured by solution calorimetry in toluene solution using dbabhNO (dbabhNO = 7-nitroso-2,3:5,6-dibenzo-7-azabicyclo[2.2.1]hepta-2,5-diene) and Ph_3SbS as chalcogen atom transfer reagents. The V−O BDE in **1**−O is 6.3 ± 3.2 kcal·mol^{-1} lower than the previously reported value for **2**−O and the V−S BDE in **1**−S is 3.3 ± 3.1 kcal·mol^{-1} lower than that in **2**−S. These differences are attributed primarily to a weakening of the V−N_{axial} bond present in complexes of **1** upon oxidation. The rate of reaction of **1** with dbabhNO has been studied by low temperature stopped-flow kinetics. Rate constants for OAT are over 20 times greater than those reported for **2**. Adamantyl isonitrile (AdNC) binds rapidly and quantitatively to both **1** and **2** forming high spin adducts of V(III). The enthalpies of ligand addition to **1** and **2** in toluene solution are −19.9 ± 0.6 and −17.1 ± 0.7 kcal·mol^{-1}, respectively. The more exothermic ligand addition to **1** as compared to **2** is opposite to what was observed for OAT and SAT. This is attributed to less weakening of the V−N_{axial} bond in ligand binding as opposed to chalcogen atom transfer and is in keeping with structural data and computations. The structures of **1**, **1**−O, **1**−S, **1**−CNAd, and **2**−CNAd have been determined by X-ray crystallography and are reported.

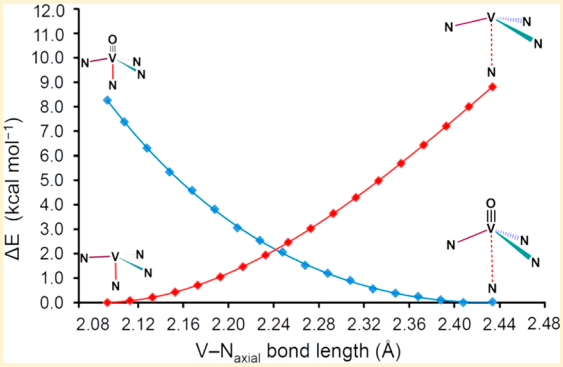

INTRODUCTION

Reversible coordination of an axial base in an octahedral metal complex has been widely studied since it plays an important role in the chemistry of cobalamin[1] and hemoglobin.[2] Recent work in the cobalamin area has resulted in isolation and structural characterization of the first "base off" adduct of vitamin B-12.[3] It is believed that the "base off" form may be the active intermediate during cobalt-alkyl bond formation. The binding of oxygen to hemoglobin and its analogs and models is also known to depend strongly on the nature of the axially coordinated base. Detailed theoretical studies show a complex range of behavior in spin state, structure, and reaction energetics, all dependent upon the nature of the specific base coordinated axially to iron.[4] In spite of considerable work, the role of axial base coordination in these complex bioinorganic systems is still not fully resolved.

Coordination of an axial base can play an important role in simpler and easier to study inorganic systems as well. In addition, rather than being based on an equatorial set of four ligands as is the case with porphyrin systems, the molecular architecture supporting a reactive metal center can be developed based on a pure X_3 ligand set,[5] and also by tripodal ligands that are formed by linking three X groups to a threefold symmetric anchor. For example, Meyer and co-workers[6] have uncovered novel CO_2 chemistry of uranium by tethering three aryloxide arms to a triazacyclononane anchor. Stack and Holm[7] reported subsite differentiation in $[4Fe\text{-}4S]^{2+}$ clusters enabled by a ligand in which three thiolate moieties were linked to the 1, 3, and 5 positions of a hexa-substituted benzene core. Deriving inspiration from the phosphatrane chemistry of Verkade,[8] the relatively bulky silyl-substituted triamidoamine ligand based upon tris(2-aminoethyl)amine (tren) was introduced to transition-metal chemistry with a report on

Received: July 24, 2014
Published: October 3, 2014

   dx.doi.org/10.1021/ic5017005 | *Inorg. Chem.* 2014, 53, 11185−11196

vanadium and titanium complexes[9] and another report on trigonal monopyramidal complexes of titanium through iron.[10] This set the stage for a rich early transition-metal chemistry of such ligands as summarized by Schrock,[11] including applications to N_2 reduction processes.[12]

Differing reactivity patterns can occur in the presence or absence of an axial base ligand, and this occurs most notably for the Mo(III) triamido complexes Mo(N[*t*-Bu]Ar)$_3$[13] and the fragment Mo(tren*) (tren* = triamidoamine ligand substituted with a range of bulky groups).[11,12] Complex Mo(N[*t*-Bu]Ar)$_3$ and the Mo(tren*) moiety both contain three trigonal anionic amido donor atoms, but the tren* complexes are augmented by a trilinked amine donor atom coordinated as an axial base. Whereas Mo(N[*t*-Bu]Ar)$_3$ does not bind N_2 to form monometallic isolable complexes, mononuclear (N_2)Mo(tren*) complexes have been isolated and characterized, and for specially constructed systems, stepwise reduction to ammonia via coupled proton transfer/electron transfer has been proven.[12] However, Mo(N[*t*-Bu]Ar)$_3$ forms a bridging μ-N_2 dinuclear complex that splits N_2 to form 2 equiv of NMo(N[*t*-Bu]Ar)$_3$.[14] Interestingly, addition of an excess of selected N-donor bases to Mo(N[*t*-Bu]Ar)$_3$ has been shown to lead to reversible binding of the N-donor and accelerated formation of [μ-N_2][Mo(N[*t*-Bu]Ar)$_3$]$_2$.[15] This may occur through formation of an intermediate base adduct (N_{base})Mo(N[*t*-Bu]Ar)$_3$ that has a greater affinity for N_2 than does Mo(N[*t*-Bu]Ar)$_3$ itself.

Three possible modes of axial base binding are shown in Scheme 1. The first case A involves reversible binding of a free base ligand in which dissociation occurs with complete loss of the coordinating base. The second case B involves a base linked by a single tethered arm that is capable of dissociation but remains in near proximity toi the metal center and is poised for rapid reassociation.[16] The final case C involves a multilinked axial base, which is present in the tren type complexes discussed above. In this case it would appear at first sight that the base could not dissociate since it is apparently locked in position by the chelate system. However, lengthening of this bond can occur with subsequent bond weakening which may approximate a "base off" position.

Scheme 1. Three Model Systems for Base (Shown as B) Activation of Trisamido Early Transition Metal Complexes[a]

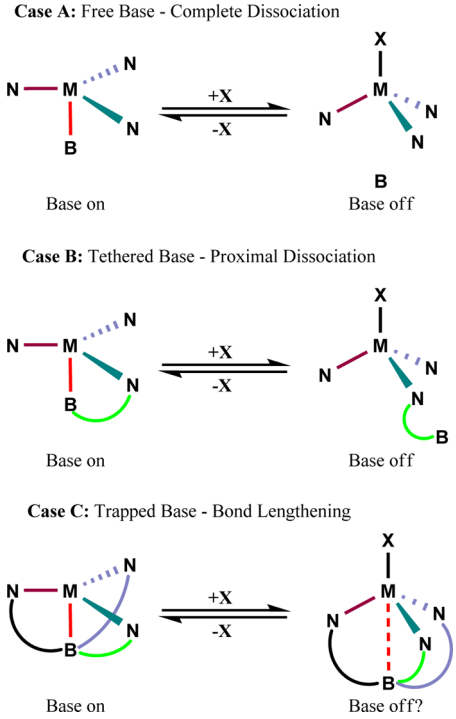

[a]Pendant groups on the amido ligands are omitted for simplicity.

This work began as an extension of our recent study[17] of oxygen atom transfer (OAT) for a series of nitrogen oxides to the complex V(N[*t*-Bu]Ar)$_3$, **2**, and comparison of its reaction energetics to that of the corresponding silylated tren complex V[(Me$_3$SiNCH$_2$CH$_2$)$_3$N], **1**.[18] Complex **2** does not contain a vacant coordination site but rather one that is blocked by close aryl contact of one of the arene ligands through the single unoccupied d orbital of V. This interaction is computed to be on the order of 4 kcal·mol^{-1}.[17] The computed structures for both species with and without this interaction have been reported previously.[17] While a crystal structure of **2** is not available, the V−arene interaction has been demonstrated crystallographically for a related complex.[19] A related Ti complex has been shown structurally to contain two such interactions at the metal center.[20] In the nomenclature of Scheme 1, complex **1** corresponds to a "trapped base" and complex **2** to a "tethered base" complex which can be viewed as a hemilabile ligand.

The presence of a similar vanadium/vanadium oxo pair (with reference to V(N[*t*-Bu]Ar)$_3$/OV(N[*t*-Bu]Ar)$_3$ (**2**/**2**−O)), namely, V[(Me$_3$SiNCH$_2$CH$_2$)$_3$N]/OV[(Me$_3$SiNCH$_2$CH$_2$)$_3$N] (**1**/**1**−O), allows direct comparison of the role of a pendant axial base for two comparable systems. In addition to OAT, sulfur atom transfer (SAT) and ligand binding of AdNC (Ad = 1-adamantyl) to **1** and **2** have also been investigated. A combination of structural, thermodynamic, kinetic, and computational studies is reported aimed at determining whether chalcogen atom transfer and ligand binding reactions are more favorable for **1** versus **2**.

2. EXPERIMENTAL SECTION

All manipulations were performed in a Vacuum Atmospheres glovebox under an inert atmosphere of purified N_2 or Ar. Solvents were obtained anhydrous and oxygen-free by sparging with N_2 and purifying using a Glass Contours Solvent Purification System (SG Water) or by distillation from Na/benzophenone under Ar. C_6D_6 was purchased from Cambridge Isotope Laboratories, degassed, and stored over activated 4 Å molecular sieves prior to use. All glassware was oven-dried at temperatures greater than 170 °C prior to use. NMR spectra were obtained on a Varian Mercury 300 MHz or Bruker Avance 400 MHz instrument equipped with Oxford Instruments superconducting magnets. **1**,[18a] SV[(Me$_3$SiNCH$_2$CH$_2$)$_3$N] (**1**−S),[18b] **2**,[21] and dbabh-NO (dbabhNO = 7-nitroso-2,3:5,6-dibenzo-7-azabicyclo[2.2.1]hepta-2,5-diene)[22] were prepared and isolated according to literature procedures, while all other reagents were acquired from commercial sources and used as received or purified by standard procedures.

2.1. Synthesis of V[(Me$_3$SiNCH$_2$CH$_2$)$_3$N] (1). In the glovebox, a 100 mL round-bottom flask containing *n*-pentane (40 mL) was charged with Li$_3$[(Me$_3$SiNCH$_2$CH$_2$)$_3$N] (1.675 g, 4.404 mmol, 1 equiv) followed by VCl$_3$(THF)$_3$ (1.639 g, 4.404 mmol, 1 equiv). The aqua-blue reaction mixture was allowed to stir for a total of 12 h, at which point it was filtered through a pad of Celite to remove liberated LiCl. The aqua-blue filtrate was then evaporated to dryness, affording a waxy blue solid. The blue solids were dissolved in *n*-pentane (3 mL), and the solution stored at −35 °C overnight to afford a crop of aqua colored X-ray quality crystals. A second crop was obtained by concentration of the remaining solution and storage at −35 °C (1.355

dx.doi.org/10.1021/ic5017005 | Inorg. Chem. 2014, 53, 11185−11196

g in 2 crops, 3.303 mmol, 75%). NMR spectral data for **1** are available in the Supporting Information.

2.2. Synthesis of OV[(Me$_3$SiNCH$_2$CH$_2$)$_3$N] (1−O). In the glovebox, solid Me_3NO (36 mg, 0.483 mmol, 1 equiv) was added to a solution of **1** (198 mg, 0.483 mmol, 1 equiv) in *n*-pentane (3 mL). The color of the reaction mixture gradually changed from aqua blue to amber over the course of 20 min. After 1 h of stirring, all volatiles were removed from the reaction mixture under reduced pressure. X-ray quality crystals of **1**−O were obtained by dissolution of the waxy amber solid in *n*-pentane (1 mL) and storage at −35 °C overnight. The remaining solution was concentrated and stored at −35 °C to obtain a second crop of crystals (138 mg in 2 crops, 0.323 mmol, 67%). NMR spectral data for **1**−O as well as **1**−S are available in the Supporting Information.

2.3. Synthesis of AdNCV[(Me$_3$SiNCH$_2$CH$_2$)$_3$N] (1−CNAd). In the glovebox, a 10 mL screw cap vial was charged with solid **1** (100 mg, 0.244 mmol, 1 equiv) followed by AdNC (39.3 mg, 0.244 mmol, 1 equiv). Then, 1 mL distilled toluene was added to the solid and the mixture was shaken for 5 min until all the solids were dissolved. The solution turned dark green in color. Then, the solution was filtered and the filtrate was poured into one side of a two-legged glass tube. The tube was sealed under vacuum. The initially empty side of the tube was kept in dry ice at −78 °C and the whole system was kept in a freezer at −20 °C. Over a period of several days there was slow transfer of toluene to the initially empty leg of the apparatus which was held at dry ice temperature. During this time dark green X-ray-quality crystals deposited on the wall of the tube. The tube containing the crystals was inverted and the toluene transferred to the other leg. The dry ice trap was replaced by a liquid nitrogen trap to freeze all the toluene and the tube containing the crystals was sealed off under vacuum. Earlier experiments had shown that even the isolated crystalline product **1**−CNAd decomposed rapidly when exposed to air. The sealed tube containing the crystals was stored in the freezer until it was taken into the glovebox for mounting. The mounted crystal in the diffractometer holder was sealed in an argon filled box and taken to the diffractometer where the apparatus was mounted under a flow of nitrogen at 100 K.

The reaction was also studied by NMR spectroscopy. In the glovebox a 1/1 mixture of AdNC and **1** was made from 50 mg **1** and 20.0 mg AdNC which were weighed in a 10 mL screw cap vial and dissolved in 1.0 mL C_6D_6. The solution was transferred into a NMR tube in the glovebox fitted with a screw cap and Teflon-lined silicone rubber septum. A NMR spectrum was taken after 10 min of the reaction. NMR spectral data of the air sensitive paramagnetic complex are available in the Supporting Information.

2.4. Synthesis of AdNCV(N[*t*-Bu]Ar)$_3$ (2−AdNC). In the glovebox, a 10 mL screw cap vial was charged with solid **2** (200 mg, 0.345 mmol, 1 equiv) followed by AdNC (56.0 mg, 0.347 mmol, 1.008 equiv). Then, 2 mL distilled toluene was added to the solid and the mixture was shaken for 5 min until all the solids were dissolved. The solution turned dark greenish brown in color. A procedure analogous to that described above for **1**−CNAd was used to isolate high quality crystals for diffraction studies. The reaction was also studied by NMR spectroscopy. In the glovebox, 50 mg **2** and 14.0 mg AdNC were weighed in a 10 mL screw cap vial and dissolved in 1.0 mL C_6D_6. The solution was transferred into an NMR tube in the glovebox fitted with a screw cap and Teflon-lined silicone rubber septum. An NMR spectrum was taken after 12 min of the reaction. NMR spectral data for the air sensitive paramagnetic complex are available in the Supporting Information.

2.5. FTIR Studies of Reaction of 1 and 2 with AdNC. In the glovebox solid AdNC (∼15 mg) and excess **1** (∼150 mg) were weighed into a screw cap vial. Two milliliters of toluene was added to the vial, which was closed and shaken until all solids had dissolved. An aliquot of the dark green solution was transferred to a CaF_2 FTIR solution cell, which was sealed and taken from the glovebox to the spectrometer. A broad band at 2133 cm^{-1} was assigned to ν-NC for **1**−CNAd. No sign of an absorbance due to free AdNC at 2129 cm^{-1} was detected. In a similar way a broad band at 2151 cm^{-1} was assigned to ν-NC for **2**−CNAd.

2.6. Chalcogen Exchange Experiments. In the glovebox, 20 mg (0.045 mmol, 1 equiv) of **1**−S and 40 mg (0.066 mmol, 1.5 equiv) of **2** were loaded into a 10 mL screw cap vial. One milliliter of toluene-d_8 was added to the solids. A ^{1}H NMR spectrum was taken after about 25 min. The NMR data showed formation of **1** and also the formation of **2**−S indicating that 'S' atom transfer had occurred. At the end of 2 h the reaction had gone nearly to completion. Investigation of the transfer in the reverse direction by reaction **1** and **2**−S showed no reaction over a similar time period. Additionally, O atom transfer between **1**−O and **2** was examined at room temperature and found to not occur in either direction using procedures identical to those described above.

2.7. Calorimetric Measurements. The enthalpy of reaction of **2** and dbabhNO was measured in a Setaram C-80 calorimeter. In the glovebox, a solution containing a large molar excess of **2** (∼0.50 g in 6 mL C_6D_6) was prepared and filtered into a clean vial. One milliliter of this stock solution was loaded into an NMR tube. The remaining 5 mL of solution was loaded into the Calvet calorimeter cell with dbabhNO (∼0.0100 g) as limiting reagent. The calorimeter cell was sealed, taken from the glovebox, and loaded into the calorimeter. Following temperature equilibration, approximately 1.5 h, the reaction was initiated and the calorimeter rotated to achieve mixing. Following the return to the baseline the calorimeter cell was taken into the glovebox, opened, and 1 mL of the solution was loaded into an NMR tube. ^{1}H NMR spectra of both the stock solution and the calorimetry solution were then acquired and the reaction was confirmed as quantitative. Four measurements done in this way yielded $\Delta H = -132.5 \pm 0.9$ kcal·mol^{-1}, which includes adjustment for the endothermic enthalpy of solution of dbabhNO in toluene (+3.8 ± 0.4 kcal·mol^{-1})[17] for a combined enthalpy in solution of $\Delta H = -136.3 \pm 1.3$ kcal·mol^{-1}. Strictly analogous procedures were used to measure other OAT and SAT reaction enthalpies.

2.8. Stopped Flow Kinetic Measurements. Toluene solutions of complex **1** and dbabhNO were prepared in an MBraun glovebox filled with ultra-high-purity argon (Airgas) and loaded into Hamilton gastight syringes. Time-resolved visible spectra were acquired at low temperatures (−80 to −62 °C) using a Hi-Tech Scientific Kinet Asyst SF-61DX2 Cryo Stopped-Flow system (TgK Scientific Ltd.) equipped with a quartz tungsten halogen light source, a J&M TIDAS diode array detector and a Brandenburg 4479 Series PMT monochromator. The instrument was equipped with stainless steel plumbing lined with PEEK tubing and a 1.00 cm^3 quartz mixing cell submerged in an ethanol cooling bath. The temperature in the mixing cell was maintained to ±0.1 °C using a CAL 3200 automatic temperature controller. Data acquisition was performed using TIDAS-DAQ and/or Kinetic Studio software programs and mixing times were 2−3 ms. All flow lines were washed extensively with Ar-saturated dry toluene prior to loading reactant solutions. Experiments were performed in a single-mixing mode of the instrument with a 1:1 (v/v) mixing ratio. Reactions were studied under pseudo-first-order conditions using excess dbabhNO. Rates of formation of **1**−O were measured by fitting kinetic traces at λ = 600 nm to a single exponential equation, rate = $-A \times \exp(-k_{obs}t) + C$ (Kinetic Studio). Observed rate constants represent an average of three measurements which gave an acceptable standard deviation (within 10%). All remaining parameters derived from kinetic data are reported with their standard deviations. All concentrations are reported after mixing in the stopped flow cell.

2.9. Computational Details. Electronic structure calculations were carried out using the BP86[23] density functional with the Stuttgart-Dresden MDF10[24] fully relativistic effective core potential and basis for V including a set of additional *f* functions and the triple-ζ quality basis set (6-311G(d,p)) for all other elements as implemented in the *Gaussian 09* suite of programs.[25] Minimum energy structures were optimized by computing analytical energy gradients. The obtained stationary points were characterized by performing energy second derivatives, confirming them as minima by the number of negative eigenvalues of the Hessian matrix of the energy. Since the computed Hessians of a couple of optimized structures were found to possess small negative eigenvalues, the zero-point vibrational effects were not included in the final energies. The V−O bond dissociation

dx.doi.org/10.1021/ic5017005 | *Inorg. Chem.* 2014, 53, 11185−11196

energies were derived by determining the enthalpy of reaction with molecular oxygen for the L_nV/L_nVO couples as previously described.[17] Alternatively, the V−S bond dissociation energies were obtained directly through the homolytic V−S dissociation reaction.

Relaxed potential energy surface scans along the $V-N_{axial}$ bond length were performed for the open-shell model complex $V[(HNCH_2CH_2)_3N]$ (in which the trimethylsilyl substituent has been replaced by H), **1m**, and for the corresponding closed-shell oxo derivative **1m**−O using the 6-311++G(3df,2p) basis set for all nonvanadium atoms.

3. RESULTS

3.1. Structural Analysis of 1, 1−O, and 1−S. Although the synthesis of **1** was reported earlier by Schrock,[18] its characterization did not include structural determination by single crystal X-ray diffraction. A slightly modified preparation and crystallization from *n*-pentane at −35 °C yielded high quality crystals of **1**, allowing for accurate determination of its structure as shown in Figure 1. The structure of **1** closely resembles that of $V[Me_2(^tBu)SiNCH_2CH_2)_3N]$ reported previously.[10]

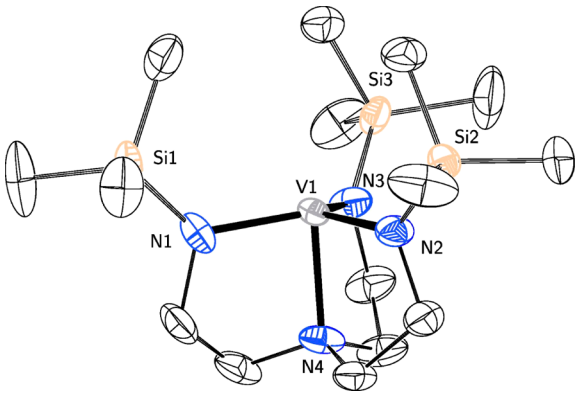

Figure 1. Solid-state molecular structure of **1** with ellipsoids at the 50% probability level rendered using PLATON.[26a] Hydrogen atoms are omitted for clarity. Selected interatomic distances (Å) and angles (deg): V1−N1 1.927(2), V1−N2 1.931(2), V1−N3 1.931(2), V1−N4 2.070(2), N2−V1−N3 119.28(8), N3−V1−N1 119.58(8), N2−V1−N1 118.85(8), N4−V1−N1 85.31(7).

Preparation of **1**−O and **1**−S proceeded by reaction of **1** with Me_3NO and S_8, respectively. Crystallization from *n*-pentane at −35 °C yielded diffraction quality crystals of **1**−O and **1**−S, whose structures are shown in Figures 2 and 3.

The V−O interatomic distance of 1.612(4) Å in **1**−O[27] is slightly longer than the 1.59 Å value estimated for the V≡O triple bond based on covalent radii.[28] The V−S interatomic distance of 2.071(1) Å in **1**−S has a value consistent with that predicted[28] for a V=S double bond of 2.06 Å. Both the V−O and the V−S bond distances are slightly longer in **1**−E than in their **2**−E (E = O, 1.590(3) Å and S 2.053(2) Å) analogues.

3.2. Synthesis and Structures of AdNC Adducts of 1 and 2. Reaction of AdNC with both **1** and **2** resulted in rapid formation of green or green-brown adducts **1**−CNAd and **2**−CNAd. NMR data (see Supporting Information) showed both to be paramagnetic high spin complexes and thus best formulated as d^2 $S = 1$ vanadium(III) complexes. FTIR data in toluene solution showed a shift to higher wavenumber than free AdNC for both adducts indicating no significant back-donation from metal to ligand: ν(AdNC) = 2129 cm^{-1}; ν(**1**−CNAd) = 2133 cm^{-1}; ν(**2**−CNAd) = 2151 cm^{-1}. The band

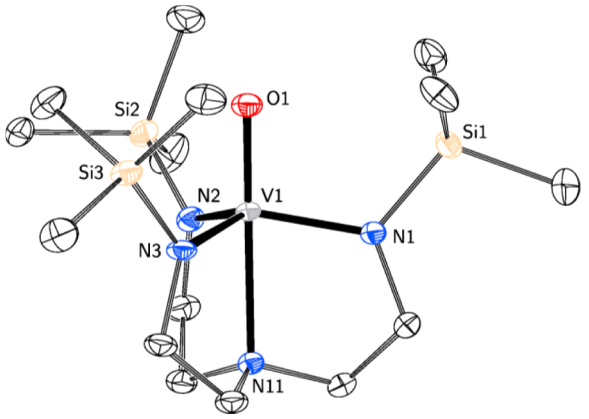

Figure 2. Solid-state molecular structure of **1**−O with ellipsoids at the 50% probability level rendered using PLATON.[26a] Hydrogen atoms are omitted for clarity. Selected interatomic distances (Å) and angles (deg) (two complexes were found in the solution denoted here with distances and angles for V1 and V2): V1−O1 1.610(2), V1−N2 1.908(2), V1−N3 1.903(2), V1−N1 1.902(2), V1−N11 2.288(2), N2−V1−N3 116.72(9), N2−V1−N1 115.19(9), N1−V1−N3 118.33(9), O1−V1−N11 177.72(8), V2−O2 1.614(2), V2−N5 1.901(2), V2−N4 1.916(2), V2−N6 1.894(2),V2−N22 2.321(2), N4−V2−N5 117.91(8), N5−V2−N6 115.92(9), N6−V2−N4 115.52(9), O2−V2−N22 177.39(8).

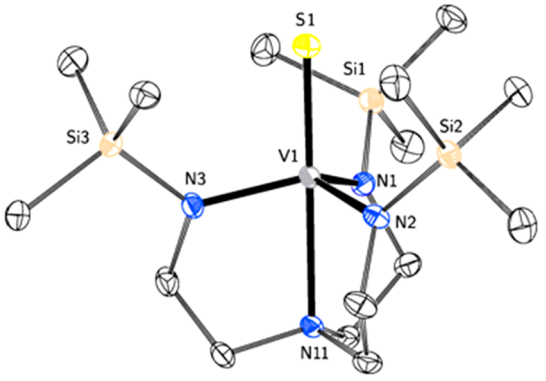

Figure 3. Solid-state molecular structure of **1**−S with ellipsoids at the 50% probability level rendered using PLATON.[26a] Hydrogen atoms are omitted for clarity. Selected interatomic distances (Å) and angles (deg): V1−S1 2.071(1), V1−N3 1.890(2), V1−N1 1.892(2), V1−N2 1.895(2), V1−N11 2.378(2), N1−V1−N3 115.92(8), N2−V1−N1 114.82(8), N2−V1−N3 115.81(8), S1−V1−N11 179.34(5), S1−V1−N3 102.26(6).

due to **2**−CNAd is broad and this may be due to different configurational isomers being present in solution. The crystal structure of **2**−CNAd (see Figure 5) reveals that in the solid state the anilide ligands adopts an arrangement where one of the three aryl rings points downward away from the bound isonitrile and two point upward toward it. This type of configuration has been found for d^2 molybdenum ketimide complexes.[29] It is plausible that in solution different rotational isomers exist in addition to that shown in the solid state.

The structures of **1**−CNAd and **2**−CNAd are shown in Figures 4 and 5 below (full structural data are available in Supporting Information).

For both complexes, the V−C−N angle is nearly linear and the C≡N distances are similar (1.155 Å for **1**−CNAd and 1.159 Å for **2**−CNAd). The C≡N distance in free AdNC has not been reported, but that in MeNC has[30] and is 1.167 Å. The

dx.doi.org/10.1021/ic5017005 | Inorg. Chem. 2014, 53, 11185−11196

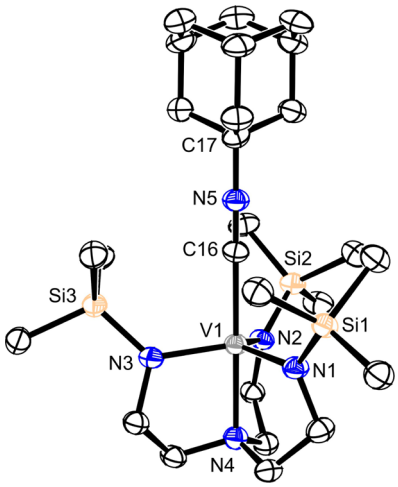

Figure 4. Solid-state molecular structure of **1**−CNAd with thermal ellipsoids drawn at the 50% probability level rendered using ORTEP.[26b] Selected interatomic distances (Å) and angles (deg): V1−N3 1.951(4), V1−N1 1.955(4), V1−N2 1.967(4), V1−C16 2.114(5), V1−N4 2.162(4), N5−C16 1.155(7), N3−V1−N1 118.47(19), N3−V1−N2 118.99(19), N1−V1−N2 118.25(19), N3−V1−C16 96.40(19), N1−V1−C16 97.13(19), N2−V1−C16 97.2(2), N3−V1−N4 83.36(17), N1−V1−N4 83.20(18), C16−V1−N4 179.7(2), C43−N10−C44 179.3(7).

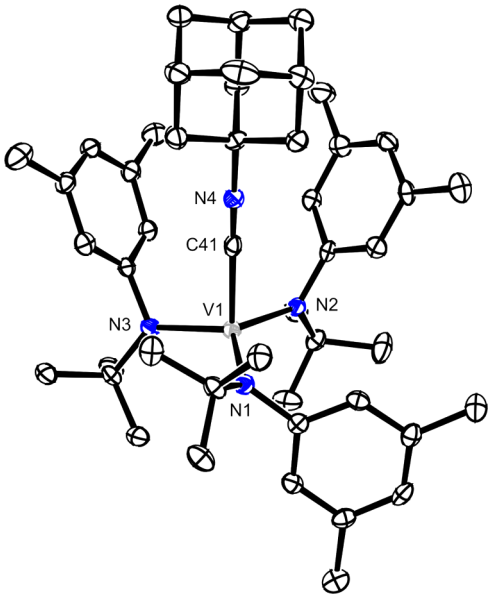

Figure 5. Solid-state molecular structure of **2**−CNAd with thermal ellipsoids drawn at the 50% probability level rendered using ORTEP.[26b] Selected interatomic distances (Å) and angles (deg): V1−N1 1.933(4), V1−N2 1.944(3), V1−N3 1.928(3), V1−C41 2.068(5), N4−C41 1.159(5), N3−V1−N1 113.94(15), N3−V1−N2 120.21(14), N1−V1−N2 121.90(14), N3−V1−C41 98.33(16), N1−V1−C41 98.82(16), N2−V1−C41 92.96(16), N4−C41−V1 177.0(4), C41−N4−C42 175.7(4).

slightly shorter C≡N distances in the adducts, coupled with the FTIR data, suggest that C≡N bond strengthening occurs upon complexation and that little donation of electron density from the d_{xz} and d_{yz} orbitals on V to vacant π^* orbitals on AdNC is present. Furthermore, the V−C bond length is 0.046 Å longer in **1**−CNAd than in **2**−CNAd analogously to what was observed for the corresponding oxo and sulfide derivatives.

3.3. Comparison of Structural Data. Selected measured and calculated structural parameters for **1**, **1**−O, **1**−S, **1**−CNAd, and **2**−CNAd are collected in Table 1. For comparative purposes, reported data for **2**−O[17] and SV(N[*t*-Bu]Ar)$_3$ (**2**−S)[31] are also shown. Upon oxidation of the vanadium center from V(+3) in **1** and **2** to V(+5) in **1**−E and **2**−E (E = O,S), the experimental and calculated interatomic distances between the vanadium atom and the three equatorial amido nitrogens shorten as expected. In contrast, a weakening of the V−N_{axial} bond occurs in **1** upon oxidation of the vanadium center, as indicated by the lengthening of the V−N_{axial} bond distances which go from 2.07 Å in **1** to 2.30 (**1**−O) and 2.39 Å (**1**−S). During this process, pyramidalization occurs at V as evidenced by a decrease in the sum of the N_{eq}−V−N_{eq} angles for the three amides. For a planar structure, Σ(N_{eq}−V−N_{eq}) would be 360° and this quantity for **1** (357.7°) indicates a nearly planar structure. The Σ(N_{eq}−V−N_{eq}) value drops to 346.5° for **1**−S and is even lower for **2**−S (331.6°). There is a good correlation between the degree of pyramidalization quantified by Σ(N_{eq}−V−N_{eq}) and the lengthening of the V−N_{axial} distance observed in all derivatives of **1** that have been structurally characterized by X-ray diffraction as shown in Figure S4 in the Supporting Information.

Alternatively, AdNC binding causes a less pronounced pyramidalization in the V(III) adducts, and consequently, the V−N_{ax} bond lengthening in **1**-CNAd is less marked than in **1**−O and **1**−S.

In addition, the three N atoms of the amido donors define a plane. Changes in the V−N_{axial} bond length in **1** comprise an upward motion of the V atom and a downward motion of the N_{axial} atom away from this plane. For **1** itself, the V atom is 0.17 Å above the plane and the N_{axial} is 1.90 Å below it. The majority of the bond lengthening that occurs upon oxidation is due to further elevation of the V atom above the plane (approximately 70%) with a minor amount (about 30%) of motion of the N_{axial} bond away from this plane due to straightening of the linking ethylene bridges. This correlation is fairly uniform for the complexes as shown in Figure S5 in the Supporting Information.

3.4. Solution Calorimetric Measurements. In order to allow direct comparison of the bond to chalcogenides for complexes **1** and **2**, the enthalpy of reaction 1 was measured in

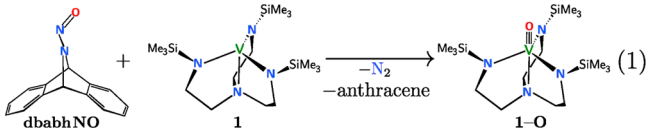

toluene solution by reaction calorimetry. Reaction 1 is rapid and quantitative as determined by NMR spectroscopy. The value ΔH_{Rxn1} = −136.3 ± 1.3 kcal·mol^{-1} compares directly to that previously reported[17] for dbabhNO and **2** of ΔH = −142.6 ± 1.9 kcal·mol^{-1} and gives a direct difference of 6.3 ± 3.2 kcal·mol^{-1} for the V−O BDEs. Based on the previous value of 154 kcal·mol^{-1} for the V−O BDE in **2**−O,[17] a value of 148 kcal·mol^{-1} is derived for the V−O BDE in **1**−O.

Likewise, the enthalpies of SAT to complexes **1** and **2** using Ph_3SbS as SAT reagent were measured as shown in eqs 2 and 3. The experimental data, ΔH_{Rxn2} = −31.0 ± 1.8 and ΔH_{Rxn3} = −34.3 ± 2.1 kcal·mol^{-1}, give a direct measure of the difference in V−S BDE of 3.3 ± 3.1 kcal·mol^{-1} with again a lower V−S BDE in **1**−S than in **2**−S. As an additional check, the chalcogen exchange reactions shown in eq 4 were investigated. In spite of

dx.doi.org/10.1021/ic5017005 | *Inorg. Chem.* 2014, 53, 11185−11196

Table 1. Comparison of Experimental and Calculated Distances (Å) and Angles (deg) for Selected Complexes[a]

	V–E		V–N_{ax}		$(V–N_{eq})_{avg}$		$\Sigma(N_{eq}–V–N_{eq})$		V–N3 plane	N_{ax}–N3 plane
	meas	calc	meas	calc	meas	calc	meas	calc	meas	meas
1	--	--	2.07	2.11	1.93	1.95	358	358	0.17	1.90
1-CNAd	2.11	2.04	2.16	2.27	1.96	1.96	356	353	0.24	1.92
1-O[b]	1.61	1.61	2.30	2.45	1.90	1.91	350	346	0.35	1.94
1-S	2.08	2.08	2.39	2.57	1.90	1.89	347	341	0.41	1.98
2	--	--	--	--	--	1.93	--	356	--	--
2-CNAd	2.07	2.00	--	--	1.94	1.95	356	353	0.23	--
2-O[c]	1.59	1.60	--	--	1.88	1.90	333	337	0.58	--
2-S[d]	2.05	2.06	--	--	1.88	1.90	332	333	0.59	--

[a]For simplicity, and to show significant changes only, distances and angles have been rounded off so that the estimated standard deviation < (1) for all data. The full data set, including ESD values, is shown in figure captions and is also available in Supporting Information. [b]For **1**–O two molecules occur in the unit cell. Within experimental error there are no differences in the bond lengths except for the V–N_{axial} bond lengths which are 2.288(2) and 2.321(2) Å. The average value in Table 1 of 2.30 therefore has an uncertainty of ±0.02 Å. [c]Data taken from ref 17. [d]Data taken from ref 31.

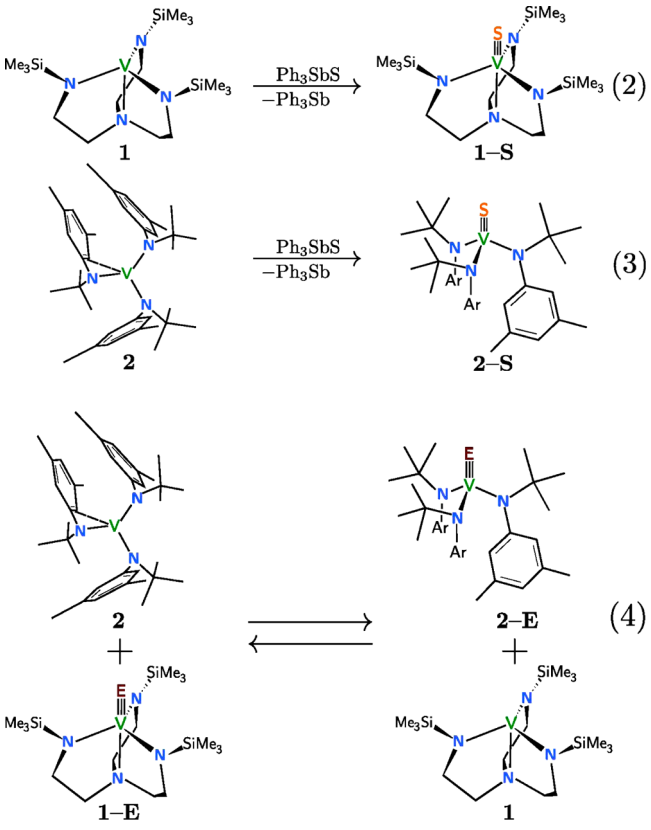

the predicted thermodynamic favorability, the OAT reaction was not observed to occur in either the forward or reverse direction. This is in keeping with the fact that OAT between $OPMe_3$ and **2** also does not occur in spite of favorable thermodynamic factors.[17] In addition, kinetic factors may also favor formation of S-bridged rather than O-bridged intermediates for steric reasons. Indeed, SAT from **1**–S to **2** producing **2**–S and **1** was observed, but only in that direction. This observation is in keeping with the generally greater tendency to form bridged species of heavier chalcogenide and pnictogen complexes.[32] In view of the small thermochemical difference predicting a higher V–S BDE in **2**–S, it gave confidence to the experimental data that reaction 4 did occur as predicted in the forward direction but not in the reverse.

The lower V–O BDE in **1**–O as compared to **2**–O prompted investigation to see if that relation carried over to simple ligand binding. Addition of AdNC to solutions of **1** and **2** results in rapid and quantitative binding. Solution calorimetric studies in toluene yielded $\Delta H = -19.9 \pm 0.6$ and $\Delta H = -17.1 \pm 0.7$ kcal·mol^{-1} for formation of **1**–CNAd and **2**–CNAd, respectively. Thus, in contrast to OAT reactivity, ligand binding studies showed that the V–C BDE in **1**–CNAd is 2.8 ± 1.3 kcal·mol^{-1} higher than in **2**–CNAd. A summary of the thermochemical BDEs derived in this work is summarized in Table 2.

Table 2. Experimental V–E (E = O, S) BDE data (kcal·mol^{-1})[a]

	1–X	2–X
V–O BDE (X = O)	148 ± 3 [148.9]	154 ± 3[17] [153.1]
V–S BDE (X = S)	98 ± 3 [96.7]	101 ± 3[17] [97.1]
V–C BDE (X = AdNC)	19.9 ± 0.6 [18.7]	17.1 ± 0.7 [18.3]

[a]Values from quantum chemical calculations are in brackets.

3.5. Kinetics of OAT from dbabhNO to 1. The kinetics of the OAT reaction between **1** and dbabhNO was studied using the stopped-flow method with spectrophotometric registration. Experiments were performed at low temperatures (−80, −71, and −62 °C) under pseudo-first-order conditions using **1** (0.5 mM) and excess dbabhNO (1.5 to 9 mM). The time-resolved spectral changes and kinetic traces at λ = 600 nm at −80 °C are shown in Figure 6. Similar to the kinetics of OAT from dbabhNO to **2**,[17] absorbance bands assignable to an intermediate adduct were not detected in the time-resolved spectra, and only clean conversion of **1** to **1**–O was observed. Due to the rapidity of the reaction, all quantitative measurements were made from data collected in single wavelength mode. At temperatures above −62 °C, the reaction rate became

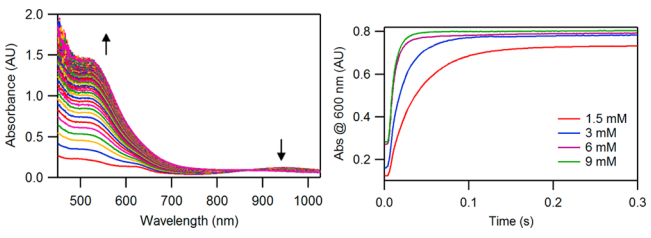

Figure 6. Left: Time resolved spectra obtained from the reaction between **1** (0.5 mM) and dbabhNO (1.5 mM) at −80 °C acquired over 1 s. Right: Kinetic traces at λ = 600 nm with varying dbabhNO concentrations at −80 °C.

dx.doi.org/10.1021/ic5017005 | Inorg. Chem. 2014, 53, 11185–11196

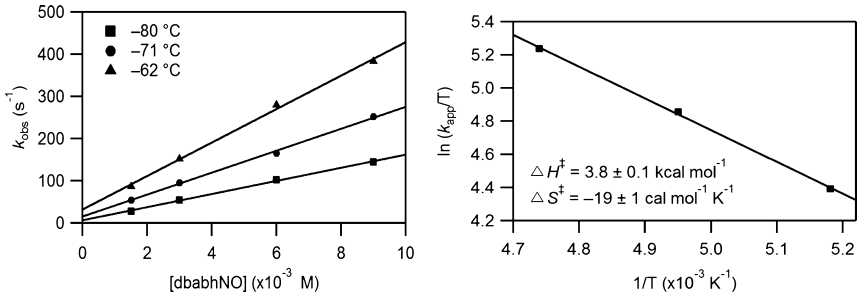

Figure 7. Left: Plots of k_{obs} versus [dbabhNO] for **1**−O formation over a temperature range of −80 to −62 °C. Right: Eyring plot with activation parameters.

too fast to measure. The formation rates of **1**−O were measured at λ = 600 nm and all kinetic traces fit well to a single exponential equation.

Observed rate constants depended linearly on [dbabhNO] and slopes of the lines yielded second order rate constants for formation of **1**−O as shown in Figure 7. Although some evidence for reversibility was observed owing to the increase in final absorbance values as [dbabhNO] increased and in the values of the *y*-intercepts as temperature rose, this was not investigated further since the observed reaction rate is reaching the limits of the stopped-flow instrument (thus the accuracy of the rate constants decreases as the reaction rates increase with increased temperature and concentrations of reagents). The accuracy of the second order rate constants reported in Table 3

Table 3. Temperature Dependent Second Order (k_{app}) Rate Constants and Activation Parameters for 1−O and 2−O Formation Measured at λ = 600 nm (1−O) or 453 nm (2−O)

	k_{app} ($\times 10^3$ $M^{-1}\cdot s^{-1}$)[a]	
T (°C)	**1**−O	**2**−O[17]
−80	15.6 ± 0.5	not measured
−71	26.0 ± 0.8	1.01 ± 0.03
−62	39.7 ± 1.5	1.82 ± 0.09
−53	too fast	3.84 ± 0.30
$\Delta H^{\ddagger}$ (kcal·mol^{-1})	3.8 ± 0.1	6.3 ± 0.3
$\Delta S^{\ddagger}$ (cal·$mol^{-1}\cdot K^{-1}$)	−19 ± 1	−13 ± 1

[a] $k_{app} = k_1k_2/(k_{-1} + k_2) = k_1/(1 + k_{-1}/k_2)$ (see ref 17 for further details).

is sufficient to quantify the rate of OAT. An Eyring plot was used to derive activation parameters ($\Delta H^{\ddagger}$ = 3.8 kcal·mol^{-1} and $\Delta S^{\ddagger}$ = −19 cal·$mol^{-1}\cdot K^{-1}$) for the OAT reaction between 1 and dbabhNO and is shown in Figure 7. Second order rate constants are provided in Table 3. While linear regression analysis gives rather low values of standard deviations for the values of $\Delta H^{\ddagger}$ and $\Delta S^{\ddagger}$ (see Figure 7), the relatively narrow temperature range accessible for kinetic experiments limits somewhat the accuracy of the derived activation parameters. Nevertheless, negative sign of activation entropy and relatively low activation enthalpy are established with confidence.

3.6. Computational Results. DFT calculations were performed to additionally check the V−E BDE values derived experimentally and to provide additional insight into the factors influencing the differing V−O BDE values for **1**−O and **2**−O. The calculated structural and energetic values are in good agreement with experimentally found values as can be seen in Tables 1 and 2. Nevertheless, calculations predict V−N_{axial} distances 0.15 and 0.18 Å longer than those observed in the solid-state molecular structures of **1**−O and **1**−S, respectively. However, as discussed below, in spite of these significant discrepancies, the energetic differences between the computed structures for **1**−O and **1**−S and the corresponding ones with a fixed V−N_{axial} bond length at the observed crystallographic values are only on the order of 1 kcal·mol^{-1}.

Structural data discussed above showed lengthening and weakening of the V−N_{axial} bond (**1**) or displacement of a weak V-arene interaction (**2**) upon oxidation of the corresponding V(III) complexes. The definition of BDEs often involves bond rearrangements,[33] which play a role in the V−O BDE in **1**−O and **2**−O. Thus, it is of utility to analyze the effect that the weakening of the V−N_{axial} bond has on reaction energetics in the oxidation of **1**. In this regard, a relaxed potential energy surface scan along the V−N_{axial} bond length was performed for the model complexes V[$(HNCH_2CH_2)_3N$], **1m**, and OV-[$(HNCH_2CH_2)_3N$], **1m**−O, in which the trimethylsilyl substituents in **1** and **1**−O have been replaced by H. Computed energies for **1m** and **1m**−O as a function of the V−N_{axial} bond length are shown in Figure 8. The computed minimum energy

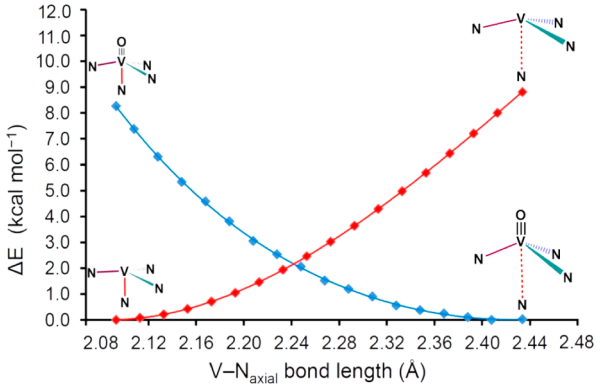

Figure 8. Change in energy with V−N_{axial} bond length for **1m** and **1m**−O. At each fixed V−N_{axial} bond length, the minimum energy structure was computed and the deviations from the minimum energy of **1m** (at 2.09 Å) and **1m**−O (at 2.43 Å) are shown. For simplicity, bridging ethylene groups have been omitted from the core structure.

configuration for **1m**−O occurs with an elongated and weakened V−N_{axial} bond at a distance of 2.43 Å, which compares with the experimental distance of 2.30 Å. As the V−N_{axial} bond length in **1m**−O moves away from its minimum value at 2.43 Å, there is less than a 1 kcal·mol^{-1} rise to the observed crystallographic value. This small energy difference may be overcome by packing forces.[34] A steeper gradient occurs as the potential energy surface rises to a value of 8.3

dx.doi.org/10.1021/ic5017005 | Inorg. Chem. 2014, 53, 11185−11196

kcal·mol^{-1} higher at a fixed V−N$_{axial}$ bond length of 2.09 Å which is the computed distance for **1m** being in good agreement with the experimental value (2.070(2) Å). Likewise, the energy dependence of **1m** as a function of the V−N$_{axial}$ bond length increases steadily to a value of 8.8 kcal·mol^{-1} at the distance of 2.43 Å, which is the computed V−N$_{axial}$ bond length for **1m**−O.

As shown in Table 3, the OAT reaction between **1** and dbabhNO is faster than the corresponding reaction with **2**. Since the first step in the OAT process is adduct formation, the LUMOs of the unsaturated vanadium(III) complexes **1** and **2** were calculated to compare the potential sites for attack by an incoming base and are shown in Figure 9. For complex **2**, the

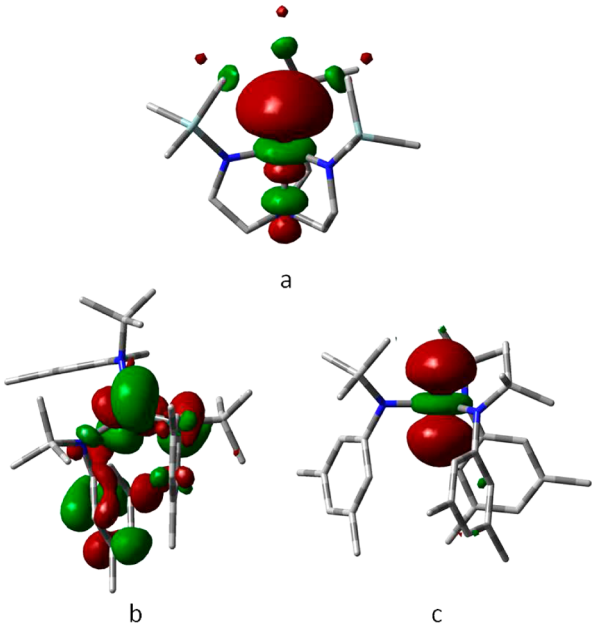

Figure 9. Computed LUMOs for **1** (a) and **2** with (b) and without (c) the weak interaction with a pendant arene.

V(III) center participates in a weak interaction with the arene group of one amido ligand as discussed earlier. For comparison purposes, the LUMO for the corresponding structure of **2** without this arene interaction was also computed. As can be seen in Figure 9, the LUMO of **1** is more accessible for attack by an OAT reagent such as dbabhNO.

3.7. NBO and NRT Analysis of a Model System. To gain a zeroth-order description of the bonding in these vanadium systems, the model open-shell complex V[(HNCH$_2$CH$_2$)$_3$N] and the corresponding closed-shell oxo and sulfido derivatives have also been geometry-optimized at the MP2 level of theory[35] using a def2-TZVPP basis set[36] as provided by the ORCA program system.[37] The structures so obtained (see Supporting Information for the optimized coordinates) are in good qualitative agreement with those determined experimentally for the trimethylsilyl derivatives, and in the analysis that follows, the focus is on gaining a qualitative understanding of the bonding. All three model systems were subjected not only to standard natural bond orbital[38] and natural population analysis[39] (NBO, NPA) to afford natural orbitals and atomic charges, but also to natural resonance theory (NRT)[40] analysis to afford values for the NRT valence (V) and bond order (b), as well as the weightings of contributing resonance structures.

Starting with the open shell (S = 1) model V[(HNCH$_2$CH$_2$)$_3$N], NRT analysis gives a total (spin α plus spin β) natural atomic valence of 3.95 at vanadium, signifying this atom's participation in four electron-pair bonds; the three amide nitrogen atoms are characterized by a valence of 3.01 (three electron-pair bonds), while the amine nitrogen enjoys a natural valence of 3.98 and should be referred to accordingly as tetravalent. The bond between vanadium and the amine nitrogen is polar in nature, being composed 89.9% of a nitrogen hybrid that is 21% s and 79% p in character (average of α and β spin). The degree of the vanadium-amide bond polarity is actually similar, but the nitrogen hybrid orbital involved in that bond type is much richer in s character (>40%). The NPA analysis is revealing in that the degree of negative charge on each amide nitrogen (−1.1) is essentially double that carried by the amine nitrogen (−0.5). The computed natural charge densities on the V atom were as follows: **1** (+1.78); **1m**−O (+1.71); **1m**−S (+1.25). Finally, we find that a single resonance structure (two unpaired electrons on V and four V−N single bonds) dominates the wave function (>50% in both α and β spin manifolds). An interesting feature of the bonding in V[(HNCH$_2$CH$_2$)$_3$N], in which the vanadium and three amide nitrogen atoms are coplanar, is the detection of three corresponding N:-V-:N three-center, four-electron hyperbonds;[41] the latter "ω bonds" disappear with the umbrella flexing of the VN(amide)$_3$ moiety that comes with addition of an axial V≡E (E = O, S) multiple bond.

On going to the oxo and sulfido derivatives, we are interested in how the bonding between vanadium and the axial amine nitrogen is affected. First, we note that the picture obtained from NPA analysis in terms of charge distribution has changed little for the nitrogen atoms (ca. −0.9 for each amide nitrogen; −0.5 for the amine nitrogen; essentially the same for oxo and sulfido). At the same time, NRT analysis gives the central metal atom a natural valence of 5.8 for both the oxo and sulfido systems, such that vanadium forms six bonds in these systems: the three metal-amide bonds, and the metal-chalcogenido triple bond (b_{VO} = 2.8, b_{VS} = 2.7). In this analysis, the tertiary amine lone pair previously (in the case of V[(HNCH$_2$CH$_2$)$_3$N]) classified as a polar bond pair now falls below the threshold cutoff to so qualify and is designated instead as an amine lone pair (see Figure 10). This is in conjunction with an increase in V−N(amine) interatomic distance of ca. 0.2−0.3 Å on going from the unsaturated vanadium(III) complex to the vanadium-(V) complexes bearing the axial metal−ligand triple bonds as discussed previously. In addition, the oxo and sulfide derivatives are not so dominated by a single Lewis structure; instead, they are more delocalized with the major Lewis structure given ca. 25% weight and all others, including ones described with a bond of the N: → (V≡E σ*) variety, accruing weight of less than ca. 5%.

Given that in these derivatives bearing a metal-chalcogen triple bond, the interaction between the tertiary amine and the vanadium center is characterized not as a first-order bond but as a second-order (hyperconjugative) interaction, it can be gauged by the energy derived for it by second-order perturbation theory analysis of the Fock matrix in the NBO basis ($\Delta E^{(2)}_{n\rightarrow\sigma^*}$):[42] 72 kcal·mol^{-1} for E = O, 80 kcal·mol^{-1} for E = S; in both cases, this particular second-order delocalization energy is the greatest of all in the molecule, the next closest in energy (ca. 40 kcal·mol^{-1}) representing amide lone pair donation into metal-amide σ* orbitals.

dx.doi.org/10.1021/ic5017005 | Inorg. Chem. 2014, 53, 11185−11196

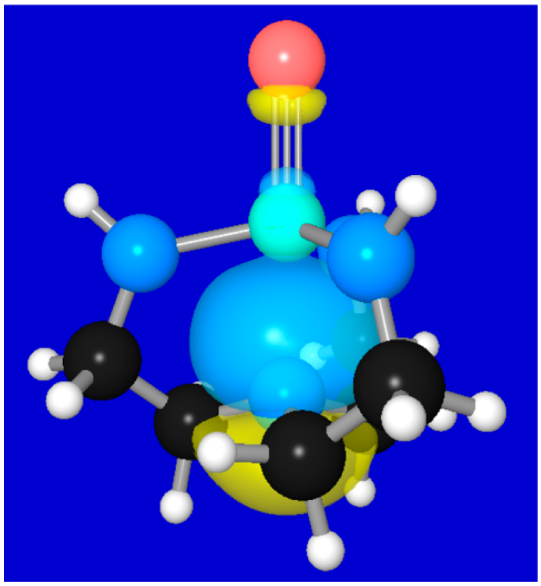

Figure 10. Natural localized molecular orbital (NLMO) corresponding to the tertiary amine lone pair of $SV[H(NCH_2CH_2)_3N]$; note the minor degree of contribution from the V≡S σ^* orbital.

4. DISCUSSION

The goal of this work is to assess the role that axial base ligation plays in the kinetics and thermodynamics of OAT, SAT, and dative ligand binding to V(III) complexes **1** and **2**, and this will be analyzed separately in the following sections.

4.1. Energetics of OAT and SAT to 1 and 2. Direct use of calorimetric data indicates that the OAT and SAT from **1** to **2** are exothermic by −6.3 ± 3.2 and −3.3 ± 3.1 kcal·mol^{-1}, respectively. The combined experimental errors are relatively large because this conclusion involves taking the difference between reactions that are individually exothermic by ∼100 kcal/mol. Competition experiments verified the relative order of thermochemical stability for the SAT reaction but for kinetic reasons did not occur in either direction for OAT. Computational studies are in relatively good agreement with the experimental data and yield the same structural and energetic trends.

The V−O and V−S BDEs are 6 and 3 kcal·mol^{-1} higher, respectively, for **2**−O and **2**−S as compared to the **1**−E complexes as can be seen in Table 2. These thermochemical differences would be enhanced by 4 kcal·mol^{-1} if the arene interaction was not present in **2**, increasing the V−O and V−S BDEs to 10 and 7 kcal·mol^{-1}, respectively. Although the V−O and V−S bond are about 0.02 Å shorter in the oxo and sulfido derivatives of **2** than in the corresponding **1**−E analogues (see Table 1), the thermochemical differences observed are higher than might be expected for this small variation on the V−E bonds.

With respect to OAT, thermochemical analysis where complete base dissociation occurs is straightforward as shown in Scheme 2.

There is a direct relationship between the relative enthalpies of OAT and base binding, since $\Delta\Delta H^{OAT} = \{\Delta H^{OAT}{}_{M\text{-}B} - \Delta H^{OAT}{}_{M}\} = \Delta\Delta H^{bind} = \{\Delta H^{bind}{}_{M=O} - \Delta H^{bind}{}_{M}\}$. Thus, the difference in enthalpies of OAT is equal to the difference in enthalpies of base binding. This kind of thermochemical analysis is common for oxidative addition reactions where the base is free to fully dissociate,[43] but is less common for a tethered or linked base adduct. Nevertheless, it is clearly applicable here as well, but rather than direct measurement of a BDE, the energy change associated with bond lengthening rather than complete breaking must be calculated.

Scheme 2. Thermochemical Cycle Comparing OAT to a Complex and Its Coordinated Base (B) Adduct[a]

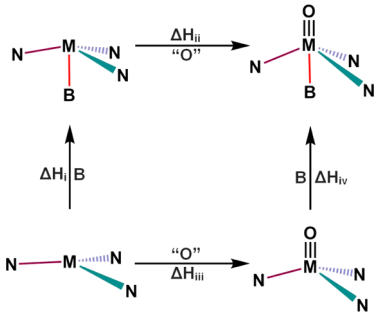

[a] $\Delta H_i = \Delta H^{\text{base binding to M}}$, $\Delta H_{ii} = \Delta H^{\text{OAT to M-B}}$, $\Delta H_{iii} = \Delta H^{\text{OAT to M}}$, and $\Delta H_{iv} = \Delta H^{\text{base binding to M≡O}}$.

In the absence of other factors, it would be expected that OAT to a metal complex with an axially coordinated base would be more exothermic than OAT to the same complex without base coordination. If the only factor to be considered was σ-donation from a "hard" N-donor base, it would be expected that the enthalpy of base binding would be higher for the higher oxidation state oxo complex than for the lower oxidation state parent complex since $\Delta\Delta H^{OAT} = \Delta\Delta H^{\text{base binding}}$. In fact, for simple gas phase ions it appears that base binding is more exothermic to the higher oxidation state metal.[44]

Experimental data for **1** and **2**, however, do not follow that expected order. When allowances are made for breaking the weak arene interaction present in **2** then OAT and SAT to **1** are 10 and 7 kcal·mol^{-1}, respectively, more exothermic for **2**. In contrast, the enthalpies of AdNC binding are more exothermic for **1** than for **2**. This is attributed to differences in the extent of weakening of the V−N_{axial} bond in **1**−CNAd and **1**−O or **1**−S. The variations in V−N_{axial} bond length observed here are in keeping with a recent redetermination of the structure of nitrosylcobalamin in which Co−N_{axial} bond length crystallographic data are summarized and show that this distance spans a range from 1.92 to 2.35 Å depending upon the specific complex.[45]

Computational results can be combined to assess the role of the V−N_{axial} bond as shown in Scheme 3. Step (e) in Scheme 3 corresponds to the thermochemically measured BDE in which **1**−O in its most stable configuration (V−N_{axial} = 2.43 Å) dissociates yielding an O atom and **1**, also in its most stable configuration (V−N_{axial} = 2.09 Å). The computed and measured data are in good agreement as discussed earlier.

Step (a) involves lengthening of the V−N_{axial} bond in **1**−O as it goes from a distance of 2.09 Å to 2.43 Å. This step is computed to be exothermic by 8.3 kcal·mol^{-1} (Figure 8). Step (c) involves shortening of the V−N_{axial} bond in **1** as it goes from a distance of 2.43 Å to 2.09 Å. This step is computed to be exothermic by 8.8 kcal·mol^{-1} (Figure 8). These data allow comparison of three OAT reactions:

A. OAT to the "base on" complex **1** to produce **1**−O also in the "base on" configuration with V−N_{axial} = 2.09 Å, as shown in step (d). This reaction is exothermic by 140.6 kcal·mol^{-1}.

dx.doi.org/10.1021/ic5017005 | Inorg. Chem. 2014, 53, 11185−11196

Scheme 3. Computed Cycle for 1−O BDE as a Function of V−N_{axial} Bond Length

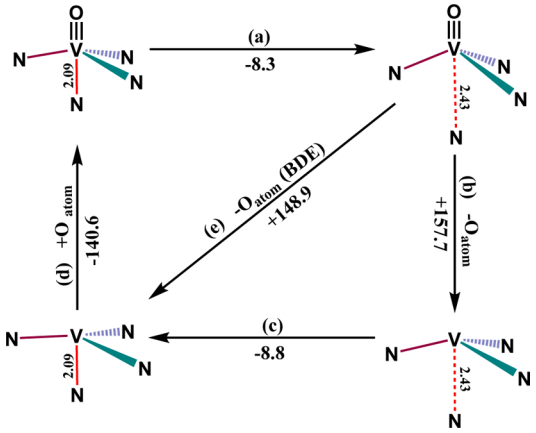

B. OAT to the "base off" complex **1** to produce **1**−O also in the "base off" configuration with V−N_{axial} = 2.43 Å, the reverse of step (b). This reaction is exothermic by 157.7 kcal·mol^{-1}.

C. OAT to the "base on" complex **1** (V−N_{axial} = 2.09 Å) to produce **1**−O in the "base off" configuration (V−N_{axial} = 2.43 Å). This corresponds to the normal BDE defined for the reaction and is shown as step (e), the reverse of which is exothermic by 148.9 kcal·mol^{-1}.

It is of interest to compare what these computed BDE data for the V−O bond would be after removing the axial base contribution to **1**−O and the arene interaction in **2**−O. As illustrated by case "B" above, the **1**−O BDE would be 157.7 kcal·mol^{-1} if the bond to the N_{axial} base was not strengthened upon deoxygenation. This is quite close to the value of 158 kcal·mol^{-1} for **2**−O if the 4 kcal·mol^{-1} arene interaction was not reformed during deoxygenation. This very close agreement may be somewhat fortuitous since the **1**−S and **2**−S BDE values differ by only 3.3 ± 3.1 kcal·mol^{-1} in spite of a greater lengthening of the V−N_{axial} bond in **1**−S than in **1**−O. The same trend is present; however, it must be recognized that experimental errors in both calorimetry and computational results are on the order of ∼3 kcal·mol^{-1} and agreement outside that range is not to be expected.

Finally, it should be noted that this type of bond lengthening upon oxidation has been observed by Kol and co-workers for conversion of V(III) to V(V)-oxo complexes chelated by an amine tris(phenolate) ligand system.[46] Bond lengthening was found to occur to an even greater extent for the amine tris(phenolate) compared to the triamidoamine system studied here. The difference in the V−N bonds in **1** (2.070 Å) and **1**−O (2.288 Å) compares to that found for the amine tris(phenolate) complexes (2.121 vs 2.4697 Å).

4.2. Qualitative Discussion of Bonding Effects in OAT to 1. The conclusion that the presence of the base serves to decrease rather than increase the V−O BDE in **1** disagrees with the intuitive argument that the V−N_{axial} bond will be stronger as the formal oxidation state of the V center increases. While this would be expected for simple gas phase systems with few ligands and a number of available orbitals, the more complex bonding picture in **1**−O shows behavior opposite of this expectation. A simplified view is that for both **1** and **2** the approximately trigonal planar structure of the amide ligands can be attributed to two forces: (1) for an ionic MX_3 complex, simple lattice energy considerations will favor a trigonal planar arrangement since deviations from that geometry bring the anionic X ligands into closer proximity without increasing the anion−cation interactions; (2) from a π-bonding perspective, the planar amides can be viewed as being sp^2 hybridized with a filled p orbital oriented to overlap with vacant orbitals on the V center. During oxidation, the V(III) complex is converted to V(V) which goes from a d^2 to a d^0 configuration. If **1**−O and **2**−O are viewed as being V(V), then π-donation from p_x and p_y orbitals on the O atom will now displace the amido π-interaction, with the result that the amido N atoms will now move down (or the V atom moves up) and rotate so that electron density that was previously involved in π-bonding to V now generates a repulsive interaction with the bonding electrons on the axial N atom. This atom will also move away, but since it is linked via relatively rigid ethylene tethers, the major motion to accommodate the V−N_{axial} bond lengthening is a motion of the V atom out of the plane of the amido ligands and toward the O atom π-donor.

In the presence of such complex rearrangements it is not strictly correct to ascribe the effects in terms of simply weakening and lengthening of the V−N_{axial} bond—there is more going on than just that. Nevertheless, it must be kept in mind that the "base on/base off" effect is ascribed to the difference between **1** and **2**. The pyramidalization effects that occur upon oxidation are similar for both **1** and **2**; in fact, **2** undergoes a more dramatic pyramidalization since it is less restricted than **1**. The presence of the axial base bond in **1** serves to inhibit pyramidalization and a balance is reached between strengthening the V−O bond and weakening the axial base bond. For purposes of simplicity these effects are covered under the blanket term "weakening of the V−N_{axial} bond".

4.3. Binding of AdNC to 1 and 2. Contrary to what was observed for OAT and SAT, the V−C BDEs in the AdNC adducts is about 3 kcal·mol^{-1} higher for **1**−CNAd than for **2**−CNAd. In spite of that, the V−C bond length is 0.046 Å shorter in **2**−CNAd, which would seem to indicate a stronger V−C bond in the latter complex. The reversal in relative thermodynamic stability of the AdNC adducts of **1** and **2** as compared to the chalcogenide species is in keeping with the role of base binding. The paramagnetic adducts **1**−CNAd and **2**−CNAd show little spectroscopic or structural signs that electron transfer has occurred. The ν(CN) stretch is shifted to higher frequency for the adducts as compared to the free isonitrile, and the AdNC bound ligand is linear. A similar observation has been made by Nocera and co-workers for a related complex.[47] In addition, the C≡NAd bond is shorter in the adducts than in the free isonitrile. This is all in keeping with formulation as the complexes are high spin V(III) adducts with little back-donation. Binding without significant electron transfer in **1** and **2** is in marked contrast to the AdNC and *t*-BuNC adducts of Mo(N[*t*-Bu]Ar)$_3$, which we have reported earlier.[48] In those adducts the ν(CN) is shifted over 400 cm^{-1} to lower frequency and the isonitrile ligand adopts a bent rather than linear geometry. In addition, the V−N_{axial} bond in **1**−CNAd is not significantly lengthened and only changes from 2.09 to 2.16 Å. As shown in Figure 8, this bond lengthening corresponds to only ∼1 kcal·mol^{-1}. In binding of AdNC to **2**, as shown in the structure in Figure 5, the V−arene interaction is fully displaced. The fact that **2** loses this interaction (4 kcal·mol^{-1}) and **1** weakens its V−N_{axial} bond (1 kcal·mol^{-1}) leads to the prediction that if the V−C BDEs in **1**−CNAd and **2**−CNAd are fundamentally the same, then **1** should be 3 kcal·

dx.doi.org/10.1021/ic5017005 | *Inorg. Chem.* 2014, 53, 11185−11196

Scheme 4. Proposed Mechanism of Reaction of 1 and dbabhNO

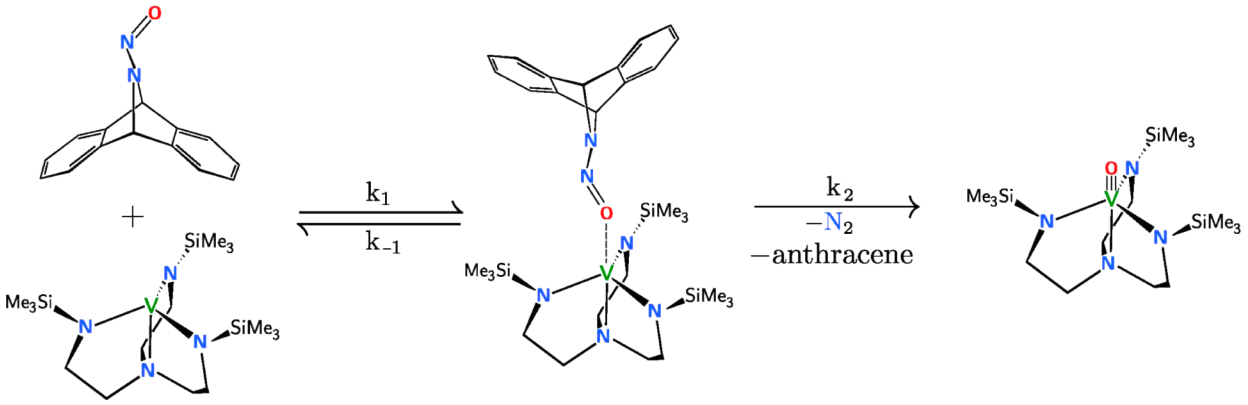

mol^{-1} more exothermic in its binding of AdNC relative to **1**. The calorimetric result of 2.8 ± 1.3 kcal·mol^{-1} is in agreement with this estimate. It should be noted that both enthalpies of binding are about 10 kcal·mol^{-1} less exothermic than that reported earlier for AdNCMo(N[*t*-Bu]Ar)$_3$.

4.4. Kinetic Differences between 1 and 2. Rapid OAT from dbabhNO to **1** results in clean formation of **1**−O, without the generation of any observable intermediates (even at temperatures as low as −80 °C). This behavior is similar to the previously reported OAT from dbabhNO to **2**,[17] such as that shown in Scheme 4 was proposed for a wide range of OAT reagents (PhNO, PyO, N_2O, and carbene adducts of N_2O or MesCNO). This general two step mechanism yielded four different subcategories of reactivity based on the relative values of the specific rate constants involved. For OAT from dbabhNO to both **1** and **2**, kinetic data are consistent with a steady state formation of an adduct between metal and substrate with no detectable buildup of intermediate in the relatively rapid reaction. The experimental value for k_{obs} in that case corresponds to $k_1k_2/(k_{-1} + k_2)$. Since there are no spectroscopic signatures detected for formation of the intermediate adduct, it is not possible to go beyond the conclusion that k_{obsd} for **1** has a rate constant approximately 20 times larger than does **2** at these low temperatures, and that it has an enthalpy of activation ∼3 kcal/mol lower. A plausible explanation for this is the more open nature of the vacant site at **1** compared to **2** as illustrated in their computed LUMOs in Figure 9.

A similar decrease in ligand binding rates of AdNC was observed for another seemingly less sterically hindered complex of molybdenum(III) (molybdaziridine hydride, Mo(H)-(Me$_2$C═NAr)(N[*i*-Pr]Ar)$_2$ compared to the three-coordinate Mo(N[*t*-Bu]Ar)$_3$).[43] In this case also, the slower rate of reaction was attributed to the necessity of generating a vacant site at the metal center prior to ligand addition. The preliminary interpretation of these kinetic results is that the slower rate of reaction of **2** compared to **1** is most likely due to a slower rate of ligand binding (k_1) with a higher enthalpy of activation due to the necessity of first cleaving the V−arene interaction in **2** to generate an available vacant site at the metal center as illustrated in the computed LUMOs in Figure 9.

5. CONCLUSIONS

The role of an axial base in influencing metal center reactivity has been widely studied for vitamin B12 and analogous complexes. In those systems, the pendant axial base is tethered loosely and a "base on/base off" equilibrium can be readily established. The current work compares structural, thermodynamic and kinetic aspects of reactivity of two V(III) trisamido complexes, both of which have an additional site blocked by a flexible ligand. Complex **2**, while formally three-coordinate, in fact has an additional site blocked by a weak interaction to a pendant arene. Complex **1** differs in that the fourth coordination site is to a tertiary amine that is part of the [(Me$_3$SiNCH$_2$CH$_2$)$_3$N] ligand itself and is "locked" in position and not able to fully dissociate. The reactions studied were OAT, SAT, and binding of AdNC. The transformations occurring during the reactions of these systems, which are relatively simple compared to more complex bioinorganic systems, are nevertheless complicated and the whole system must be analyzed as "one piece of cloth". Several conclusions applicable to complexes **1** and **2** are as follows:

1. The "intrinsic" V−O BDEs in these systems are on the order of 158 kcal·mol^{-1}, and this is decreased by ∼4 kcal·mol^{-1} in **2**−O by establishment of a weak V−arene interaction and by ∼9 kcal·mol^{-1} in **1**−O by establishment of a stronger V−N$_{axial}$ interaction upon deoxygenation.

2. Upon OAT and SAT to **1**, there is significant lengthening and weakening of the V−N$_{axial}$ bond and computational studies indicate that this polar bond pair present in **1** is better described instead as an amine lone pair with a minor degree of N:→(V≡E σ^*) second-order contribution in complexes **1**−O and **1**−S.

3. In contrast to OAT and SAT, ligand addition of AdNC is more exothermic to **1** than to **2**, in spite of **2**−CNAd having a shorter V−C bond length than **1**−CNAd. A plausible explanation for this observation is the fact that binding of AdNC to **1** only slightly weakens and lengthens the V−N$_{axial}$ bond in **1**, while AdNC binding to **2** results in complete loss of the V−arene interaction exhibited by **2**.

4. In spite of being less thermodynamically favorable, OAT occurs more rapidly to **1** than it does to **2** due to the more open nature of the vacant axial site opposite the donor axial amine. This is reflected primarily in the greater enthalpy of activation for addition to **2** due to the necessity of breaking the weak V−arene interaction.

5. For highly exothermic oxidative addition reactions such as OAT and SAT, the 6−9 kcal·mol^{-1} thermochemical differences associated with weakening of the V−N$_{axial}$ bond does not significantly change the reaction energetics. For reactions more nearly thermoneutral, however, it could play a significant role and alter the reaction profile.

dx.doi.org/10.1021/ic5017005 | *Inorg. Chem.* 2014, 53, 11185−11196

■ ASSOCIATED CONTENT

Supporting Information

Additional experimental details including NMR spectroscopic data, full crystallographic data, and additional computational data. This material is available free of charge via the Internet at http://pubs.acs.org.

■ AUTHOR INFORMATION

Corresponding Authors

*E-mail: elena.rybak-akimova@tufts.edu.
*E-mail: manuel.temprado@uah.es.
*E-mail: captain@miami.edu.
*E-mail: ccummins@mit.edu.
*E-mail: c.hoff@miami.edu.

Notes

The authors declare no competing financial interest.

■ ACKNOWLEDGMENTS

This material is based upon work supported by the National Science Foundation under Grants CHE-1362118 (C.C.C.), CHE-1412909, CHE-1229426, CHE-0750140 (E.R.A.), CHE-0615743 (C.D.H), the Spanish Ministry of Economy and Competitiveness (MINECO) under CTQ2012-36966 (M.T.), and award of a GAANN fellowship (T.P.).

■ REFERENCES

(1) (a) Randaccio, L.; Brancatelli, G.; Demitri, N.; Dreos, R.; Hickey, N.; Siega, P.; Geremia, S. *Inorg. Chem.* **2013**, *52*, 13392. (b) Hamza, M. S. A.; Zou, X.; Banka, R.; Brown, K. L.; van Eldik, R. *Dalton Trans.* **2005**, 782. (c) Rovira, C.; Biarnes, X. *Inorg. Chem.* **2004**, *43*, 6628.

(2) Kharitonov, V. G.; Sharma, V. S.; Magde, D.; Koesling, D. *Biochemistry* **1997**, *36*, 6814.

(3) Moore, T. C.; Newmister, S. A.; Rayment, I.; Escalante-Semerena, J. C. *Biochemistry* **2012**, *51*, 9647.

(4) Liao, M.; Huang, M.; Watts, J. D. *J. Phys. Chem. A* **2010**, *114*, 9554.

(5) (a) Cummins, C. C. *Prog. Inorg. Chem.* **1998**, *47*, 685. (b) Green, M. L. H. *J. Organomet. Chem.* **1995**, *500*, 127.

(6) (a) Castro-Rodriguez, I.; Nakai, H.; Zakharov, L. N.; Rheingold, A. L.; Meyer, K. *Science* **2004**, *305*, 1757. (b) Castro-Rodriguez, I.; Meyer, K. *J. Am. Chem. Soc.* **2005**, *127*, 11242.

(7) Stack, T. D. P.; Holm, R. H. *J. Am. Chem. Soc.* **1988**, *110*, 2484.

(8) Verkade, J. G. *Acc. Chem. Res.* **1993**, *26*, 483.

(9) Cummins, C. C.; Schrock, R. R.; Davis, W. M. *Organometallics* **1992**, *11*, 1452.

(10) Cummins, C. C.; Lee, J.; Schrock, R. R.; Davis, W. M. *Angew. Chem., Int. Ed.* **1992**, *31*, 1501.

(11) Schrock, R. R. *Acc. Chem. Res.* **1997**, *30*, 9.

(12) Schrock, R. R. *Acc. Chem. Res.* **2005**, *38*, 955.

(13) Laplaza, C. E.; Odom, A. L.; Davis, W. M.; Cummins, C. C.; Protasiewicz, J. D. *J. Am. Chem. Soc.* **1995**, *117*, 4999.

(14) Cherry, J.-P. F.; Johnson, A. R.; Baraldo, L. M.; Tsai, Y.-C.; Cummins, C. C.; Kryatov, S. V.; Rybak-Akimova, E. V.; Capps, K. B.; Hoff, C. D.; Haarand, C. M.; Nolan, S. P. *J. Am. Chem. Soc.* **2001**, *123*, 7271.

(15) Tsai, Y. C.; Cummins, C. C. *Inorg. Chim. Acta* **2003**, *345*, 63.

(16) This can also be viewed as a "hemilabile" ligand: Slone, C. S.; Weinberger, D. A.; Mirkin, C. *Prog. Inorg. Chem.* **1999**, *48*, 233.

(17) Palluccio, T. D.; Rybak-Akimova, E. V.; Cai, X.; Majumdar, S.; Chui, M.; Temprado, M.; Silvia, J. S.; Cozzolino, A. F.; Tofan, D.; Cummins, C. C.; Captain, B.; Hoff, C. D. *J. Am. Chem. Soc.* **2013**, *135*, 11357.

(18) (a) Cummins, C. C.; Schrock, R. R. *Inorg. Chem.* **1994**, *33*, 395. (b) Cummins, C. C.; Schrock, R. R.; Davis, W. M. *Inorg. Chem.* **1994**, *33*, 1448.

(19) Ruppa, K. B. P.; Desmangles, N.; Gambarotta, S.; Yap, G.; Rheingold, A. L. *Inorg. Chem.* **1997**, *36*, 1194.

(20) Wanandi, P. W.; Davis, W. M.; Cummins, C. C.; Russell, M. A.; Wilcox, D. E. *J. Am. Chem. Soc.* **1995**, *117*, 2110.

(21) Brask, J. K.; Fickes, M. G.; Sangtrirutnugul, P.; Durà-Vilà, V.; Odom, A. L.; Cummins, C. C. *Chem. Commun.* **2001**, 1676.

(22) Carpino, L. A.; Padykula, R. E.; Barr, D. E.; Hall, F. H.; Krause, J. G.; Dufresne, R. F.; Thoman, C. J. *J. Org. Chem.* **1988**, *53*, 2565.

(23) (a) Becke, A. D. *J. Chem. Phys.* **1993**, *98*, 5648. (b) Perdew, J. P. *Phys. Rev. B* **1986**, *33*, 8822.

(24) Dolg, M.; Wedig, U.; Stoll, H.; Preuss, H. *J. Chem. Phys.* **1987**, *86*, 866.

(25) Frisch, M. J. et al. *Gaussian 09*, revision C.01; Gaussian, Inc.: Wallingford, CT, 2010.

(26) (a) Spek, A. L. *J. Appl. Crystallogr.* **2003**, 7. (b) Farrugia, L. J. *J. Appl. Crystallogr.* **2012**, *45*, 849.

(27) This reflects the average of 1.610(2) and 1.614(2) for the V−O distances in the two molecules in the unit cell.

(28) Pyykkö, P.; Atsumi, M. *Chem.—Eur. J.* **2009**, *15*, 12770.

(29) Curley, J. J.; Sceats, E. L.; Cummins, C. C. *J. Am. Chem. Soc.* **2006**, *128*, 14036.

(30) The CN bond length of MeNC(g) is 1.167 Å as determined by microwave absorption spectroscopy. Kessler, M.; Ring, H.; Trambarudo, R.; Gordy, W. *Phys. Rev.* **1950**, *79*, 54.

(31) Brask, J. K.; Durà-Vilà, V.; Diaconescu, P. L.; Cummins, C. C. *Chem.Commun.* **2002**, 902.

(32) Johnson, M. J. A.; Lee, P. M.; Odom, A. L.; Davis, W. M.; Cummins, C. C. *Angew. Chem., Int. Ed.* **1997**, *36*, 87.

(33) For example cleaving the C═C bond of ketene (H_2C═C═O) produces H_2C and C≡O. The formal definition of the C═C bond in ketene is lower than expected since the C═O bond is converted to a C≡O concomitantly with C═C bond cleavage. See: Blanksby, S. J.; Ellison, G. B. *Acc. Chem. Res.* **2003**, *36*, 255.

(34) Thompson, H. P. G.; Day, G. M. *Chem. Sci.* **2014**, *5*, 3173.

(35) Møller, C.; Plesset, M. S. *Phys. Rev.* **1934**, *46*, 618.

(36) Weigend, F.; Ahlrichs, R. *Phys. Chem.* **2005**, *7*, 3297.

(37) Neese, F. *WIREs Comput. Mol. Sci.* **2012**, *2*, 73.

(38) (a) Glendening, E. D.; Landis, C. R.; Weinhold, F. *WIREs Comput. Mol. Sci.* **2012**, *2*, 1. (b) Glendening, E. D.; Badenhoop, J. K.; Reed, A. E.; Carpenter, J. E.; Bohmann, J. A.; Morales, C. M.; Landis, C. R.; Weinhold, F. *NBO 6.0*; http://nbo6.chem.wisc.edu/; Theoretical Chemistry Institute; University of Wisconsin, Madison, WI, 2013. (c) Glendening, E. D.; Landis, C. R.; Weinhold, F. *J. Comput. Chem.* **2013**, *34*, 1429.

(39) Reed, A. E.; Weinstock, R. B.; Weinhold, F. *J. Chem. Phys.* **1985**, *83*, 735.

(40) (a) Glendening, E. D.; Weinhold, F. *J. Comput. Chem.* **1998**, *19*, 593. (b) Glendening, E. D.; Weinhold, F. *J. Comput. Chem.* **1998**, *19*, 610. (c) Glendening, E. D.; Badenhoop, J. K.; Weinhold, F. *J. Comput. Chem.* **1998**, *19*, 628.

(41) Weinhold, F.; Landis, C. R. *Discovering chemistry with natural bond orbitals*; Wiley: Hoboken, NJ, 2012.

(42) Weinhold, F.; Landis, C. R. *Valency and bonding: a natural bond orbital donor-acceptor perspective*; Cambridge University Press: Cambridge, U.K., 2005.

(43) Hoff, C. D. *Prog. Inorg. Chem.* **1992**, *42*, 503.

(44) Nose, H.; Rogers, M. T. *ChemPlusChem* **2013**, *78*, 1109.

(45) Hassanin, H. A.; El-Shahat, M. F.; DeBeer, S.; Smith, C. A.; Brasch, N. E. *Dalton Trans.* **2010**, *39*, 10626.

(46) Groysman, S.; Goldberg, I.; Goldschmidt, Z.; Kol, M. *Inorg. Chem.* **2005**, *44*, 5073.

(47) Groysman, S.; Villagrán, D.; Freedman, D. E.; Nocera, D. G. *Chem. Commun.* **2011**, *47*, 10242.

(48) Stephens, F. H.; Figueroa, J. S.; Cummins, C. C.; Kryatova, O. P.; Kryatov, S. V.; Rybak-Akimova, E. V.; McDonough, J. E.; Hoff, C. D. *Organometallics* **2004**, *23*, 3126.